

Broad-Spectrum Allosteric Inhibition of Herpesvirus Proteases

Jonathan E. Gable,^{†,§} Gregory M. Lee,[†] Priyadarshini Jaishankar,[‡] Brian R. Hearn,[‡] Christopher A. Waddling,^{||} Adam R. Renslo,^{†,‡} and Charles S. Craik*,[†]

[†]Department of Pharmaceutical Chemistry, University of California, San Francisco, California 94158-2280, United States

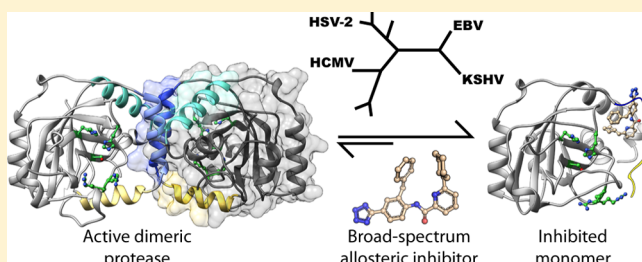
[‡]Small Molecule Discovery Center, University of California, San Francisco, California 94158-2250, United States

[§]Graduate Group in Biochemistry and Molecular Biology, University of California, San Francisco, California 94158-2280, United States

^{||}Department of Biochemistry and Biophysics, University of California, San Francisco, California 94158-2280, United States

Supporting Information

ABSTRACT: Herpesviruses rely on a homodimeric protease for viral capsid maturation. A small molecule, DD2, previously shown to disrupt dimerization of Kaposi's sarcoma-associated herpesvirus protease (KSHV Pr) by trapping an inactive monomeric conformation and two analogues generated through carboxylate bioisosteric replacement (compounds 2 and 3) were shown to inhibit the associated proteases of all three human herpesvirus (HHV) subfamilies (α , β , and γ). Inhibition data reveal that compound 2 has potency comparable to or better than that of DD2 against the tested proteases. Nuclear magnetic resonance spectroscopy and a new application of the kinetic analysis developed by Zhang and Poorman [Zhang, Z. Y., Poorman, R. A., et al. (1991) *J. Biol. Chem.* 266, 15591–15594] show DD2, compound 2, and compound 3 inhibit HHV proteases by dimer disruption. All three compounds bind the dimer interface of other HHV proteases in a manner analogous to binding of DD2 to KSHV protease. The determination and analysis of cocrystal structures of both analogues with the KSHV Pr monomer verify and elaborate on the mode of binding for this chemical scaffold, explaining a newly observed critical structure–activity relationship. These results reveal a prototypical chemical scaffold for broad-spectrum allosteric inhibition of human herpesvirus proteases and an approach for the identification of small molecules that allosterically regulate protein activity by targeting protein–protein interactions.



Herpesviruses make up one of the most prevalent viral families, including nine human types that cause a variety of severe illnesses and are classified into three subfamilies.¹ The α subfamily of human herpesviruses (HHVs) includes herpes simplex viruses 1 and 2 (HSV-1 and HSV-2, respectively), as well as Varicella Zoster virus (VZV). The β subfamily includes human cytomegalovirus (HCMV) and human herpesviruses 6a, 6b, and 7 (HHV-6a, -6b, and -7, respectively). Lastly, the γ subfamily includes Epstein-Barr virus (EBV) and Kaposi's sarcoma-associated herpesvirus (KSHV). All currently approved treatments for herpesvirus infection target viral DNA replication. However, these drugs suffer from poor efficacy because of viral resistance mutations, the requirement of frequent intravenous injection, or severe dose limiting side effects such as myelosuppression or nephrotoxicity. For these reasons, there has been a prevailing interest in alternative potential therapeutic targets for herpesvirus infection.²

All human herpesviruses share a structurally and functionally conserved serine protease (Pr) that is critical in the formation of the mature capsid and is allosterically activated through dimerization.¹ Genetic deletion of this viral Pr in HSV-1 precluded capsid maturation, confirming that the protease is necessary for successful viral replication and validating the

enzyme as a potential therapeutic target.³ Similarly, knockdown of the maturational Pr in murine cytomegalovirus (MCMV), a model of β herpesvirus infection, causes a significantly reduced viral load.⁴ The critical role that these proteases play in the viral replication cycle and their conservation across the HHVs make them potential therapeutic targets.

Initial attempts to exploit HHV proteases as therapeutic targets were directed at the active site. These relied heavily on chemical “warheads” for covalent inhibition and/or peptidomimetic scaffolds.^{5,6} Despite some *in vitro* success, efforts to target the active site of these essential serine proteases have yet to yield inhibitors ready to advance into the clinic.^{5,7–11} Structural evidence helps explain the need for covalent inhibitors and the lack of pharmacologically viable lead compounds. All HHV proteases have a relatively shallow substrate binding pocket with a strict preference for alanine at P1 and serine at P1'. In addition, substrate binding is reported to occur through an induced-fit mechanism.^{12–15} Being both shallow and dynamic, this active site is particularly challenging to inhibit.

Received: March 14, 2014

Revised: June 21, 2014

Published: June 30, 2014



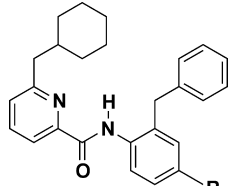
Through studying the structure–function relationships of these enzymes, researchers built up an understanding of their allosteric regulation.^{6,12,13,16–26} Each monomer has an independent active site.¹ In the monomeric state, the enzyme is inactive and partially disordered. As the dimer, the enzyme is active, and the disordered C-terminal residues of the monomer form two helices, one that functions as a major contact surface at the dimer interface and one that interacts with the catalytic site. This disorder-to-order transition links the dimer interface to the catalytic site.^{16,27} Given the evidence supporting an allosteric link between Pr dimerization and activation, we have focused our efforts on identifying molecules that target the dimer interface.^{6,12,16,22,23,28} In doing so, we previously identified a small molecule inhibitor of KSHV Pr designated DD2 [compound 1 (Table 1)].^{29,30}

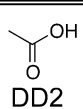
DD2, a benzyl-substituted 4-(pyridine-2-amido)benzoic acid, is a helical peptide mimetic and allosteric inhibitor that prevents the disorder-to-order transition that activates KSHV Pr, thus trapping an inactive monomeric state.^{27,30} The primary DD2 binding pocket, ~15 Å from the active site, is formed by conformational changes that occur only in the partially

disordered monomer. The pocket forms when Trp109, an aromatic hot spot in the core of the protein, changes rotameric state.²⁷ The presence of a conserved aromatic hot spot in all nine human herpesvirus proteases suggests the potential for the development of broadly antitherapeutic small molecules that allosterically inhibit HHV Pr enzyme activity by disrupting protein–protein interactions.

We set out to determine whether DD2 or analogues thereof could be pan allosteric inhibitors of herpesvirus proteases. To accomplish this, we generated a series of compounds in which the carboxylate of DD2 was replaced with polar nonionic or polar anionic functional groups (Table 1) and assessed the inhibitory activity of the compounds. These new analogues and DD2 were evaluated with respect to their potency and mechanism of action against a panel of representative HHV proteases spanning all HHV subfamilies: HSV-2 (α), HCMV (β), EBV (γ), and KSHV (γ) proteases. Binding of an inhibitor to KSHV Pr was characterized using our repertoire of nuclear magnetic resonance (NMR) assays as well as X-ray crystallographic studies, which established the mechanism of action and binding site at atomic resolution.²⁷ To facilitate more rapid determination of the mechanism of inhibition, particularly where NMR and crystallographic approaches are not readily available, we applied a kinetic analysis that distinguishes between dissociative (i.e., dimer disruption) and nondissociative inhibitors of obligate dimeric enzymes. This analysis was first described and conducted for dimer disruptors of HIV-1 Pr by Zhang and Poorman.³¹ Cumulatively, this approach allowed the development of improved inhibitors and detailed analysis of the inhibition of this highly dynamic protein–protein interface.

Table 1



| R | KSHV Pr IC ₅₀ (μM) |
|---|-------------------------------|
|  | 1.5 ± 0.3 |
|  | 1.0 ± 0.1 |
|  | 3.7 ± 0.7 |
|  | No inhibition |
|  | No inhibition |
|  | No inhibition |
|  | No inhibition |

MATERIALS AND METHODS

Materials. Buffer and solvent components were purchased from VWR or Fisher Scientific at >99% purity. The P6 peptide substrate (PVYtBuQA-ACC) was purchased crude (AnaSpec, Inc.) and purified via reverse-phase high-performance liquid chromatography on a C¹⁸ column as described previously.³² The P4 peptide substrate, YtBuQA-ACC, was synthesized and purified as previously described, but using the Symphony Quartet multiple synthesizer (Protein Technologies, Inc.) for the addition of the last three amino acids.³²

Protein Expression and Purification. Expression and purification of the KSHV, HCMV, HSV-2, and EBV proteases and their respective isoleucine-to-valine and truncated variants were conducted as previously described.^{27,33} Primer sequences are listed in the Supporting Information.

Acquisition and Analysis of NMR Data. All protein NMR data were acquired at 27 °C on a Bruker Avance 500 MHz spectrometer equipped with a QCI CyroProbe and a B-ACS 60-slot autosampler. Protease sample concentrations, buffer conditions, data acquisition, and data processing were as previously described.^{27,30} NMR characterization of the small molecule inhibitors is described in the Supporting Information under Analog Synthesis.

Determination of Kinetic IC₅₀ Values. IC₅₀ values were determined as previously described with the following modifications.³⁰ A 2-fold dilution series of the compound was prepared in 100% DMSO from 10 to 0.156 mM and/or from 5 to 0.078 mM. The P6 substrate concentrations were 5, 65, 150, and 30 μM for KSHV, EBV, HCMV, and HSV-2 proteases, respectively. For KSHV, EBV, and HCMV proteases, the final enzyme concentration was 1 μM in assay buffer [25 mM potassium phosphate (pH 8), 150 mM KCl, 0.1 mM EDTA,

and 1 mM dithiothreitol (DTT)] with a final DMSO concentration of 2%. HSV-2 protease assays were conducted at a final enzyme concentration of 10 μM in the assay buffer described above, supplemented with 10% glycerol and 500 mM sodium citrate. HSV-2 Pr has very low activity and requires large amounts of an antichaotropic agent to induce dimerization and activation.²⁶ Data were acquired from a Spectra MAX Gemini EM fluorescence microplate reader (Molecular Devices) using excitation and emission wavelengths of 380 and 460 nm, respectively. The initial velocity was used to calculate percent activity, which was plotted versus inhibitor concentration and fit to eq 1 using IGOR Pro (WaveMetrics, Inc.). Y , U , L , C , and H correspond to the percent activity, maximal percent activity, minimal percent activity, inhibitor concentration, and Hill slope, respectively. All IC_{50} values are reported as the mean \pm the standard deviation ($n = 3$).

$$Y = U + \frac{U - L}{1 + 10^{(\log \text{IC}_{50} - \log C)H}} \quad (1)$$

Previously reported IC_{50} values for DD2 against KSHV Pr were determined with the concentration of substrate (S_0) used for screening, a value approximately 10-fold greater than the K_M (P6 substrate $K_M = 11 \pm 3 \mu\text{M}$; $S_{0,\text{prev}} = 100 \mu\text{M}$).³⁰ Herein, reported IC_{50} values were obtained at $S_0 = 0.5 - 1 \times K_M$ for all enzymes unless explicitly stated otherwise. Substrate-induced dimerization has been reported for KSHV Pr whereby an excess of substrate drives the monomer–dimer equilibrium toward the dimeric state, decreasing the apparent potency of dimer disruptors.⁶ This explains why the KSHV IC_{50} value for DD2 reported herein is somewhat lower than that previously reported.

Zhang–Poorman Analysis. The analysis of Zhang and Poorman is based on Scheme 1 and eqs S1 and S2 of the Supporting Information, which describe the linear relationship between $E_0/\sqrt{k_{\text{exp}}}$ and $\sqrt{k_{\text{exp}}}$ under first-order kinetics for inhibited and apo conditions, where E_0 is the total enzyme concentration and k_{exp} is the experimental first-order rate constant.³¹ The enzyme concentration is varied while the initial substrate concentration, S_0 , is held constant with or without inhibitor.

Data collection was conducted in black round-bottom polystyrene 96-well plates (Corning) with reaction volumes of 100 μL in assay buffer (described above). The substrate concentration was optimized for each enzyme to achieve first-order reaction kinetics. For EBV and HCMV proteases, the initial concentration of the P6 substrate was 15 μM . The K_M for KSHV Pr and P6 substrate is approximately 11 μM .³⁰ This relatively low K_M value prevented us from achieving $S_0 \ll K_M$ while still having substrate in large excess of enzyme. To achieve the conditions described above, we synthesized a shorter substrate, P4 (YtBuQA-ACC), with a K_M of 80 μM , allowing us to satisfy the constraints imposed by Zhang–Poorman analysis. For KSHV Pr, 15 μM P4 substrate was used. Concentrated enzyme stocks were diluted into assay buffer in siliconized Eppendorf tubes to reach concentrations of 1–4.6 μM for all proteases, with final concentrations determined by a Hewlett-Packard 8453 UV-vis spectrometer (1 cm path length). Inhibitor was added from a stock in 100% DMSO, with a final assay DMSO concentration of 2%. Enzyme and inhibitor were incubated at room temperature for 45 min and then dispensed into the 96-well plate. Addition of 5 μL of a substrate stock in 10% DMSO was used to start the reaction, resulting in a final DMSO concentration of 2.5%. Reactions

were conducted at room temperature, and data were acquired as described above. Full kinetic curves were recorded for the majority of reactions and fit to a single exponential using IGOR Pro (WaveMetrics, Inc.) to determine k_{exp} . For high inhibitor concentrations, with low enzyme concentrations the signal remained linear and a full curve could not be recorded, even over a 7 h time course. In these cases of low activity, we utilized the relationship $k_{\text{exp}} = v_0/S$ to calculate k_{exp} from the initial velocity, where v_0 is the initial velocity and S is the substrate concentration determined from total hydrolysis. The use of v_0 as a substitute for k_{exp} was noted by Zhang and Poorman and has been used successfully elsewhere.^{31,34} The dependent variable ($E_0/\sqrt{k_{\text{exp}}}$) is plotted as a function of $\sqrt{k_{\text{exp}}}$ for each inhibitor concentration and fit to a line in accordance with eqs S1 and S2 of the Supporting Information.³¹

Acquisition of X-ray Crystallography Data and

Determination of Structure. Stock KSHV Pr $\Delta 196$ solutions for crystallography were prepared at a concentration of 7 mg/mL in 100 mM KCl, 0.07 mM EDTA, 16.5 mM KP_i (pH 8.0), and 0.66 mM DTT. Inhibitor was added to the stock protein solution to a final concentration of 1 mM (3.4-fold molar excess, final DMSO concentration of 9%) and incubated at 30 °C for 30 min. The protein/inhibitor solution was added in a 1:1 ratio to the reservoir solution, and crystals were grown at 17 °C with the hanging drop vapor diffusion method. Initial crystallization hits were identified using the MCGS2 sparse matrix screen (Microlytics) and subsequently optimized by grid screening. The final reservoir solution for compound 2 cocrystallization consisted of 0.1 M sodium acetate (pH 7.8), 0.88 M NaH₂PO₄, 1.32 M K₂HPO₄, and 0.2 M KCl. For compound 3, the reservoir solution contained 0.1 M imidazole (pH 8), 0.4 M NaH₂PO₄, 1.6 M K₂HPO₄, and 0.1 M NaCl. Crystals appeared after 14–30 days as small rectangular prisms. For compound 2, a 1.45 Å resolution data set was collected from a 0.2 mm × 0.05 mm × 0.05 mm crystal. In the case of compound 3, a 2.15 Å resolution data set was collected from a smaller crystal measuring 0.1 mm × 0.03 mm × 0.03 mm. Data were collected at Lawrence Berkeley National Laboratory Advanced Light Source beamline 8.3.1 using a crystal flash-cooled to 100 K in mother liquor with 12% glycerol as the cryoprotectant. Further details of the X-ray diffraction data processing and analysis are described in the Supporting Information. Resulting structures of compounds 2 and 3 in complex with truncated KSHV protease were deposited in the Protein Data Bank (PDB) as entries 4P3H and 4P2T, respectively.

Structural figures within this paper and the Supporting Information were created using UCSF Chimera version 1.8.1. Chimera is developed by the Resource for Biocomputing, Visualization, and Informatics at the University of California, San Francisco (supported by National Institute of General Medical Sciences Grant P41-GM103311).

Modeling Using the Protein Local Optimization

Program (PLOP). MarvinSketch version 5.11.3 (ChemAxon) was used to generate mol2 files for compounds 2 and 3 based on the PDB coordinates determined from their cocrystal structures. PLOP (M. Jacobson, <http://www.jacobsonlab.org>) was used to optimize the entire monomer–ligand complex and structural waters within 10 Å of the ligand using the opt boolean followed by the minim side and minim res commands.^{35–37} OPLS-AA 2005 force field parameters for compounds 2 and 3 were generated using the hetgrp_ffgen

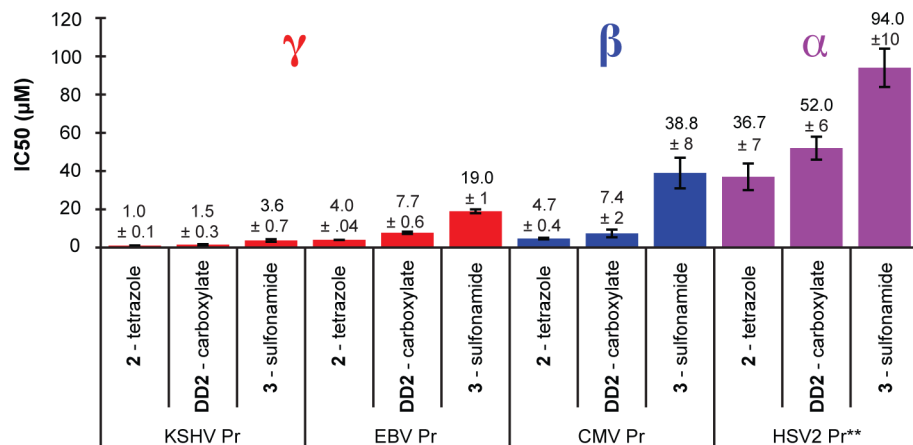


Figure 1. IC₅₀ values across multiple HHV proteases. IC₅₀ values for DD2 and compounds 2 and 3 against KSHV, EBV, HCMV, and HSV-2 proteases. Two asterisks for HSV-2 indicate values were determined with a buffer and enzyme concentration different from those used for all other enzymes (Materials and Methods).

command from Schrodinger with mol2 files from MarvinSketch as input.

RESULTS

A Scaffold for Broad-Spectrum Allosteric Inhibition of Human Herpesvirus Proteases. DD2, compound 2, and compound 3 inhibit HCMV (β), EBV (γ), HSV-2 (α), and KSHV (γ) proteases with micromolar potencies (Figure 1). KSHV Pr, the HHV Pr used in the discovery of DD2, was the most potently inhibited enzyme with IC₅₀ values of $1.0 \pm 0.1 \mu\text{M}$ for compound 2, $1.5 \pm 0.3 \mu\text{M}$ for DD2, and $3.6 \pm 0.7 \mu\text{M}$ for compound 3 (Figure 1). All compounds bearing a polar but nonionic substitution for the carboxylate of DD2 [compounds 4–7 (Table 1)] showed no inhibition of KSHV Pr, although some of these analogues exhibit poor solubility at low micromolar concentrations. For example, compounds 5 and 7 were found by dynamic light scattering to form large aggregates ($>80 \text{ nm radii}$) at $1 \mu\text{M}$. These results suggest limited concentrations of the free compound are available in solution under such conditions, precluding conclusions about the SAR. Compounds 4 and 6, however, did not form large aggregates but were inactive (Figure S1 and methods of the Supporting Information). Overall, the data for compounds 2–7 suggest the importance of an anionic group at the position of the carboxylate in DD2 for inhibition.

The compounds developed here had the lowest potency against HSV-2 Pr, with IC₅₀ values ranging from ~ 37 to $94 \mu\text{M}$ (Figure 1). This may be in part due to the high concentration of enzyme and antichaotropic agents necessary for activity with this enzyme (Materials and Methods). While DD2 inhibits HCMV and EBV proteases with similar potencies (IC₅₀ values of 7.4 ± 2 and $7.7 \pm 0.6 \mu\text{M}$, respectively), compound 3 inhibits HCMV Pr with an IC₅₀ of $39 \pm 8 \mu\text{M}$ and EBV with an IC₅₀ of $19 \pm 1 \mu\text{M}$. Compound 2 is more potent than either DD2 or compound 3 against HCMV and EBV proteases (IC₅₀ values of 4.7 ± 0.4 and $4.0 \pm 0.1 \mu\text{M}$, respectively). It is noteworthy that the IC₅₀ values for these enzymes are similar to the total enzyme concentration used. This may indicate tight binding; however, analysis of tight-binding inhibition is confounded by the monomer–dimer equilibrium in our system. The IC₅₀ value for DD2 against KSHV protease is similar at 395 and 1300 nM total enzyme, suggesting stoichiometric inhibitor binding is not the only determinant of IC₅₀. For all

enzymes, compound 2 was most potent, followed by DD2 and finally compound 3. While broad-spectrum inhibition of herpesvirus proteases is apparent from these data, the mechanism of inhibition cannot be inferred from IC₅₀ data. We therefore applied Zhang–Poorman analysis to determine whether a consistent mechanism of inhibition was operating across Pr family members. For this analysis, we used our most potent inhibitor, compound 2, as a representative of the inhibitor class.

Application of Zhang–Poorman Analysis in Investigating Dimer Disruption of Human Herpesvirus Proteases. Zhang and Poorman developed a kinetic approach for determining whether an obligate dimeric enzyme, HIV-1 Pr, is inhibited by a dissociative mechanism (dimer disruption) or a nondissociative mechanism (Scheme 1 and eq 1 of the Supporting Information) using a plot of $E_0/\sqrt{k_{\exp}}$ (y-axis) versus $\sqrt{k_{\exp}}$ (x-axis) with and without inhibitor. This plot is generated by measuring the experimental first-order rate constant (k_{\exp}) with varied enzyme (E_0) and inhibitor concentrations as described in Materials and Methods.³¹ When dimer disruption is the dominant mode of inhibition, an increasing inhibitor concentration results in an increasing y-intercept that scales as $1 + [I]/K_i$, where $[I]$ is the total concentration of the inhibitor and K_i is the dissociation constant of the inhibitor–monomer complex (eq 1 of the Supporting Information).³¹ Zhang–Poorman analysis provides orthogonal mechanistic data based solely on enzyme kinetics, complementing our NMR-based assays.

Application of this analysis to KSHV Pr and our known dimer disruptor, DD2, provided a positive control and illustrates the effectiveness of this analysis for HHV proteases. As expected, increasing concentrations of DD2 resulted in increasing y-intercepts, indicating higher apparent dissociation constants for the dimer [$K_{d,\text{app}}$ (Figure 2b)]. For strictly dissociative inhibition where K_i is relatively small and on the order of the inhibitor concentration, the competitive (K_c) and noncompetitive (K_c') dissociation constants are very large, and the noncompetitive rate constant (k_{cat}') is small, the slope of these plots simplifies to $(k_{\text{cat}}/K_M)^{-1}$ and should be constant across all inhibitor concentrations (Scheme 1 and eq 2 of the Supporting Information).³¹ The slope we observe decreases slightly with an increasing DD2 concentration. This observation is consistent with mixed-type inhibition previously reported for

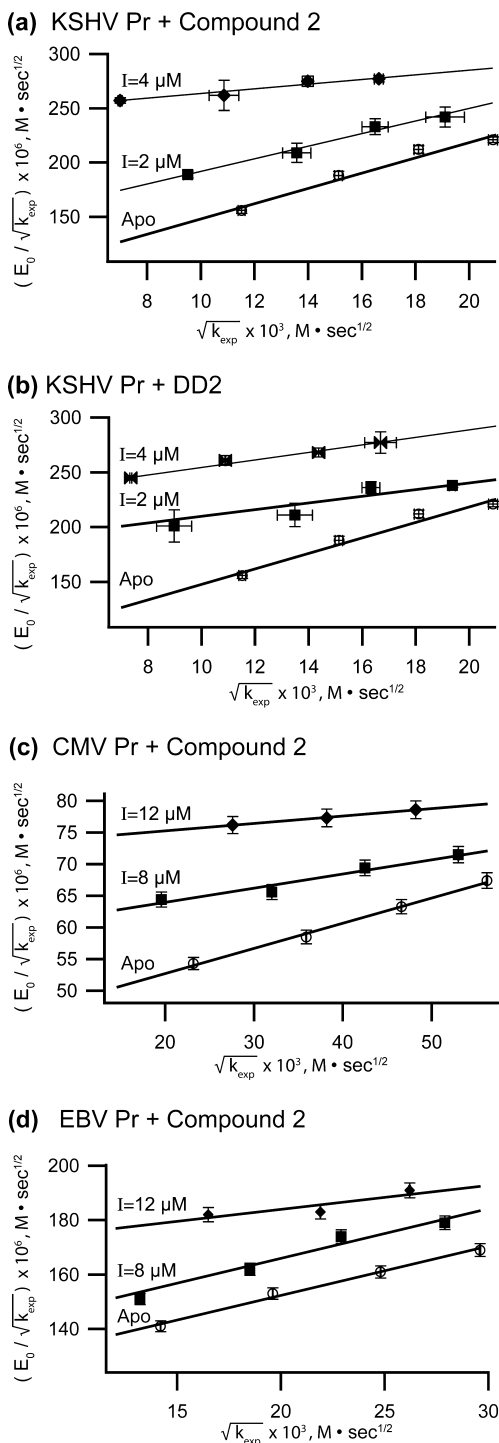


Figure 2. Zhang–Poorman analysis of DD2 and compound 2. Against KSHV protease, both compound 2 (a) and DD2 (b) show an increasing intercept with an increasing inhibitor concentration, indicative of dimer disruption. The same trend is observed for compound 2 with HCMV (c) and EBV (d) proteases.

this inhibitor.³⁰ A decrease in slope with an increasing inhibitor concentration indicates $K_c/K'_c > 1$ and $K_c > K'_c$, suggesting the dimer–substrate–inhibitor complex is more dominant than the dimer–inhibitor complex in contributing to mixed inhibition (derivation in the Supporting Information). This illustrates how Zhang–Poorman analysis can reveal both the more subtle noncompetitive inhibition (K'_c) and the diagnostic increase in

the y -intercept indicative of dimer disruption (dissociative inhibition).

We applied this analysis to our new inhibitor compound 2 against our panel of HHV proteases. HSV-2 Pr had too little activity to reliably perform the kinetic analysis under the required first-order conditions and so was excluded from analysis. Zhang–Poorman analysis of compound 2 for the other three proteases (KSHV, EBV, and HCMV) is fully consistent with a mechanism of dimer disruption. In each case, increasing concentrations of compound 2 result in increased y -intercepts and $K_{d,app}$ values (Figure 2a,c,d). Mixed inhibition was also observed for compound 2, indicated by a decreasing slope with an increasing inhibitor concentration.

Compounds 2 and 3 Disrupt Dimerization by Binding the Dimer Interface Core Analogously across All HHV Protease Subfamilies. Application of $^{13}\text{C}-\text{H}$ HSQC spectroscopy using selectively [$^{13}\text{C}-\epsilon\text{-methyl}$]methionine-labeled KSHV Pr allowed for more direct structural confirmation that compounds 2 and 3 disrupt dimerization. Met197 in helix 5 of KSHV Pr is directly involved in monomer–monomer interaction (Figure 3a,c). The monomer–dimer equilibrium of KSHV Pr exhibits slow exchange on the NMR time scale, giving rise to distinct Met197 monomer and Met197 dimer resonances in the HSQC spectrum. It was previously shown that the addition of DD2 results in the loss of the Met197 dimer peak and a chemical shift perturbation in the Met197 monomer peak, diagnostic of dimer disruption.³⁰ Addition of equimolar amounts of compound 2 or 3 has a similar effect with a complete loss of the dimer peak and a shift in the Met197 monomer peak [$\Delta\delta_{total(compound 2)} = 0.095$ ppm, and $\Delta\delta_{total(compound 3)} = 0.049$ ppm (Figure 3b)]. These data provide further support for the conclusion drawn from Zhang–Poorman analysis though fall short of defining the site of binding for these inhibitors.

To determine whether our new inhibitors 2 and 3 bind at the dimer interface, we first performed selective [$^{13}\text{C}-\delta 1\text{-methyl}$]-isoleucine labeling for analysis by $^{13}\text{C}-\text{H}$ HSQC spectroscopy. Like we did for KSHV Pr–DD2 interactions, we hypothesized that binding of compounds 2 and 3 would take place at the conserved putative aromatic hot spot of each enzyme and be largely independent of the two C-terminal helices. This led us to design a truncated obligate monomeric construct of HSV-2 Pr analogous to those previously reported for KSHV and HCMV proteases [KSHV Pr Δ196 and HCMV Pr Δ221, respectively (Figures 3a and 4b,d, pink)]. For HSV-2 Pr, a stop codon was introduced at residue 214, leaving two turns of helix 5 and completely removing helix 6 to generate HSV-2 Pr Δ213 (Figures 3a and 4f, pink). Selective [$^{13}\text{C}-\delta 1\text{-methyl}$]isoleucine labeling provided a set of NMR probes for monitoring binding at the dimer interface near the aromatic hot spot. In addition to selective labeling, the large majority of $^{15}\text{N}-\text{H}$ HSQC resonances for KSHV Pr have been reported previously, including that of the side chain indole ring of Trp109.²⁸ Perturbation of the dimer interface residue Trp109 resonance provides additional support for binding at the dimer interface hot spot.

Addition of a >5-fold molar excess of compound 2 or 3 to KSHV Pr Δ196 yielded resonance perturbations in both the $^{13}\text{C}-\text{H}$ and $^{15}\text{N}-\text{H}$ HSQC spectra indicative of binding at the dimer interface in the same pocket bound by DD2 (Figure 4a and Figure S3 of the Supporting Information). All seven isoleucines of KSHV Pr Δ196 are resolved in the $^{13}\text{C}-\text{H}$ HSQC spectrum and were previously assigned.²⁷ The crystal

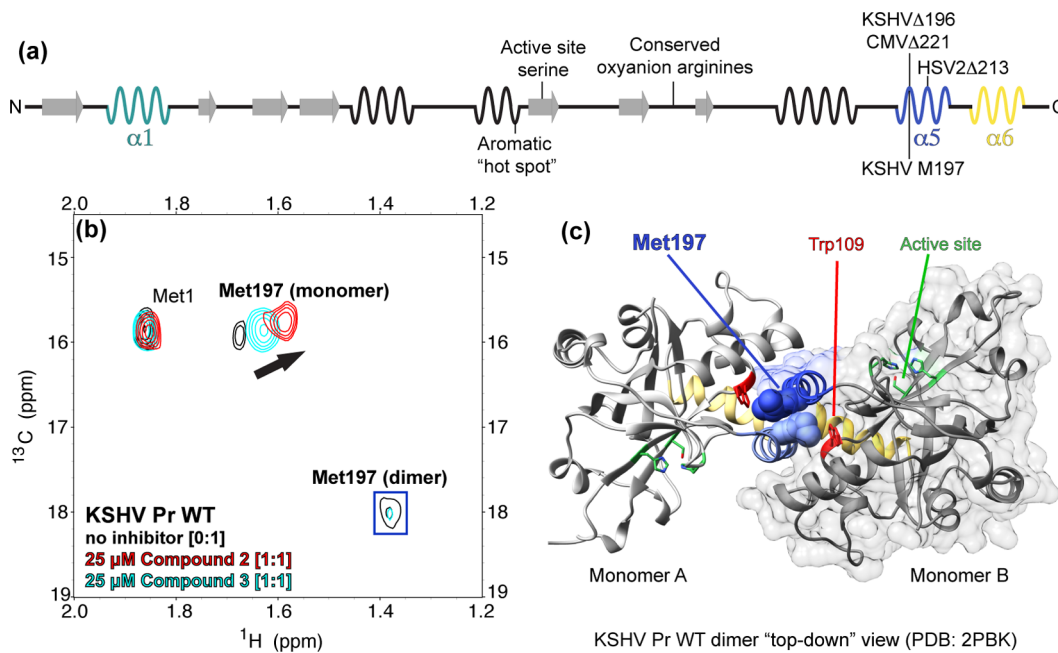


Figure 3. HHV domain diagram and ^{13}C - ^1H HSQC spectrum of KSHV protease with selectively labeled Met197. HHVs share a common structure consisting of seven β strands and six major helices. Helices 1 (cyan) and 5 (blue) are major components of the dimer interface. Helices 5 and 6 (yellow) undergo a disorder-to-order transition upon dimerization. The locations of the aromatic hot spot residues (KSHV W109, HCMV Y128, EBV W111, and HSV2 Y124), active site serines (KSHV S114, HCMV S132, EBV S116, and HSV2 S129), conserved oxyanion arginines (KSHV R142 and R143, HCMV R165 and R166, EBV R147 and R148, and HSV2 R156 and R157), and sites of truncation are indicated. (a) Met197 exhibits distinct resonances for the dimeric and monomeric states of KSHV Pr. The spectral overlay of the apo form (black), 1 molar equiv of compound 3 (cyan), and 1 molar equiv of compound 2 (b) shows addition of either compound results in a reduction in the Met197 dimer peak intensity as well as a chemical shift perturbation and an increase in the intensity of the Met197 monomer peak. The Met1 peak remains unperturbed. The location of Met197 at the dimer interface (c) is shown on the wild-type dimeric KSHV protease crystal structure (PDB entry 2PBK) in the proximity of the aromatic hot spot residue Trp109.

structure of DD2 bound to KSHV Pr Δ 196 shows that Ile44 and Ile105 contribute hydrophobic surface area to the DD2 pocket and are closest to the aromatic hot spot residue Trp109 [≤ 5 Å (Figure 4b)]. Therefore, binding of a small molecule to the DD2 pocket is expected to most significantly perturb resonances corresponding to Ile44 and Ile105 while leaving the five remaining isoleucine peaks largely unperturbed. Indeed, in the presence of compound 2, Ile44 and Ile105 exhibit significant peak shifts [for Ile44, $\Delta\delta_{\text{total}} = 0.078$ ppm; for Ile105, $\Delta\delta_{\text{total}} = 0.094$ ppm (Figure S2 of the Supporting Information)]. Compound 3 binding and positive control DD2 exhibit similar effects [for Ile44, $\Delta\delta_{\text{total(compound 3)}} = 0.063$ ppm and $\Delta\delta_{\text{total(DD2)}} = 0.060$ ppm; for Ile105, $\Delta\delta_{\text{total(compound 3)}} = 0.120$ ppm and $\Delta\delta_{\text{total(DD2)}} = 0.087$ ppm (Figure 5 and Figure S2 of the Supporting Information)]. Ile44 also exhibits substantial peak broadening for all compounds. Addition of DD2, compound 2, or compound 3 causes extensive peak broadening of the Trp109 indole HN ^{15}N - ^1H HSQC resonance, further supporting the conclusion that DD2, compound 2, and compound 3 bind the same transient allosteric pocket at the dimer interface (Figure S3 of the Supporting Information).

NMR was utilized to map the binding of a small molecule to truncated HCMV Pr (HCMV Pr Δ 221). HCMV Pr Δ 221 contains only two isoleucines, Ile61 and Ile96, assigned by isoleucine-to-valine mutations (Figure 4d and Figure S5 of the Supporting Information). In the wild-type dimer crystal structure, Ile61 and Ile96 are located ~ 5 and ~ 9 Å from the putative aromatic hot spot Tyr128, respectively (Figure 4d, PDB entry 1CMV). Addition of an approximately 10-fold

molar excess of compound 2 or 3 to HCMV Pr Δ 221 resulted in peak broadening of both the Ile61 and Ile96 probes (Figures 4c and 5d). A comparable effect was observed for the addition of DD2 at the same relative concentration (Figure 5c). The decrease in peak volume was greater for compound 2 than for compound 3 with both isoleucine probes. For all three inhibitors, exchange peak broadening is consistent with binding to HCMV Pr.

^{13}C - ^1H HSQC experiments suggest compounds 2 and 3 also bind at the dimer interface of HSV-2 Pr. The truncated HSV-2 Pr construct (HSV-2 Δ 213) contains nine isoleucine residues (Figure 4f), which were assigned by isoleucine-to-valine mutations (Figure S4 of the Supporting Information). Addition of DD2, compound 2, or compound 3 causes substantial peak broadening for the Ile21 and Ile57, and to a lesser extent Ile86 and Ile121, peak resonances (Figures 4e and 5e,f). Ile21, Ile86, and Ile121 are predicted to be in the proximity of the putative hot spot residue Tyr124 (PDB entry 1AT3). The observation that the resonance of Ile57 is also perturbed indicates a change in the electronic environment farther from the predicted binding site, consistent with changes in conformational equilibria in the presence of a compound or binding to multiple sites. In total, the NMR experiments described here suggest that DD2, compound 2, and compound 3 bind the dimer interface across representative members of all HHV Pr subfamilies. For KSHV Pr Δ 196 cocrystallized with compound 2 or 3 confirms at atomic resolution that these compounds bind the same pocket as DD2 and adopt similar conformations (see below).

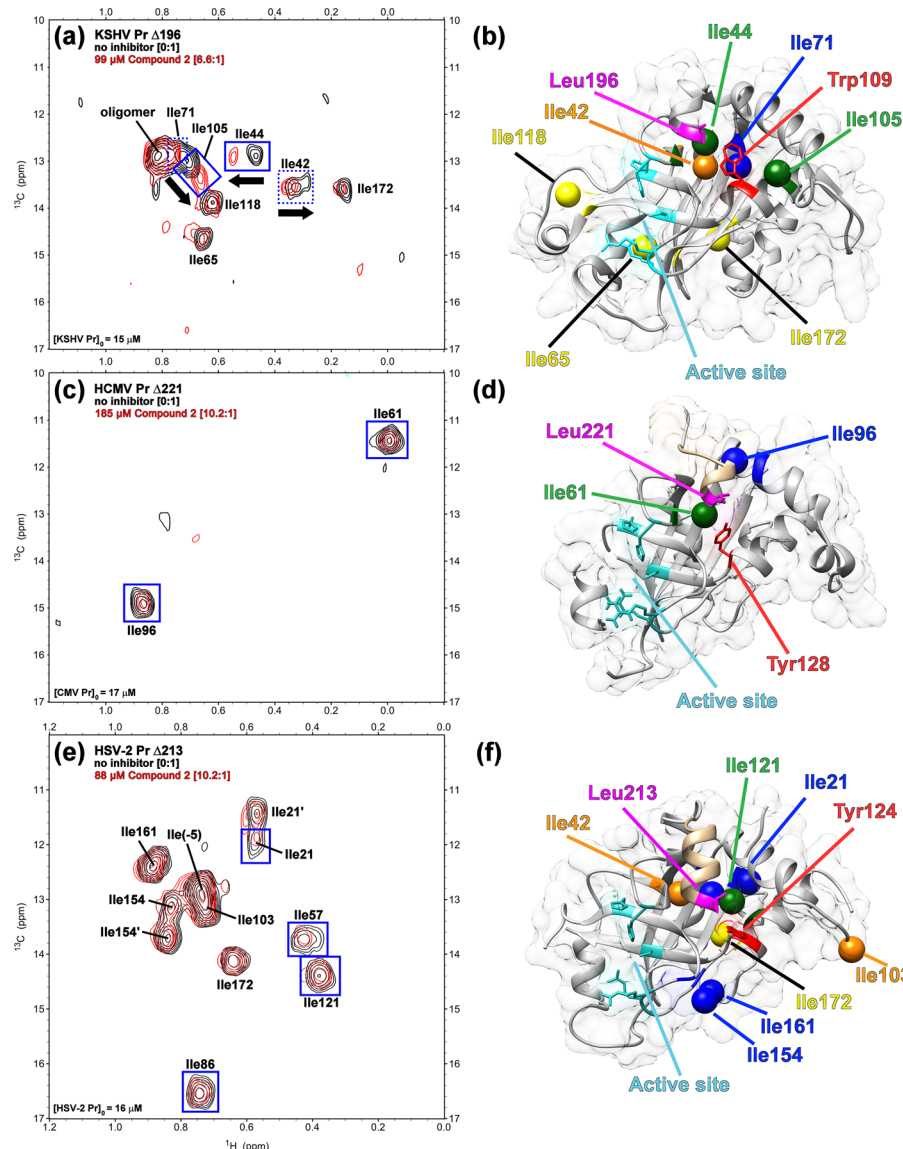


Figure 4. $^{13}\text{C}-^1\text{H}$ HSQC Ile spectra in the presence of compound 2. The $^{13}\text{C}-^1\text{H}$ HSQC spectra of selectively $^{13}\text{C}-^1\text{H}$ [$\delta 1$ -methyl]isoleucine-labeled truncated constructs KSHV Pr $\Delta 196$ (a), HCMV Pr $\Delta 221$ (c), and HSV-2 Pr $\Delta 213$ (e) in the presence of 0 (black) and 5–10 molar equiv of compound 2 (red) indicate compound 2 binds at the dimer interface across representative members of all three herpesvirus subfamilies. Prime signs denote minor conformer peak resonances. The locations of isoleucine $\delta 1$ -methyl groups in the KSHV (b), HCMV (d), and HSV-2 (f) truncated constructs are shown at the dimer interface, and color-coded with respect to the distance to the putative aromatic hot spot (red). Isoleucine residues within 5 Å (green), 5–10 Å (blue), 10–15 Å (orange), and >15 Å (yellow) are indicated. Helix 5 (tan), the active site (cyan), and the point of truncation (pink) are also denoted.

Cocrystals with Compounds 2 and 3 Confirm the Mode of Binding and Explain Structure–Activity Relationships. The discovery that an anionic group is required for inhibitory activity is not clearly explained by the DD2–KSHV Pr Δ196 cocrystal structure or other prior studies.^{27,30} To improve our understanding of the SAR for this compound series and to establish the effect of bioisosteric replacement on binding to KSHV protease at an atomic level, we pursued cocrystallization studies of KSHV Pr Δ196 with compounds 2 and 3.

Compounds **2** and **3** cocrystallized with KSHV Pr Δ196 to yield 1.45 and 2.15 Å resolution structures, respectively (PDB entry 4P3H for compound **2** and PDB entry 4P2T for compound **3**). The two structures overlay with a $\text{C}\alpha$ rmsd of 0.25 Å. Comparison to the KSHV Pr Δ196–DD2 cocrystal structure (PDB entry 3NQJ) gives a $\text{C}\alpha$ rmsd of 0.3 Å for both.

Structures with compounds **2** and **3** have an asymmetric unit containing two truncated monomers, each with largely the same conformation [$C\alpha$ rmsd $\sim 0.8 \text{ \AA}$ (Figure 6)]. A noteworthy difference between the two monomers is the position of the C-terminal residues, which are in the proximity of the inhibitor. Residues Val190 and onward diverge in backbone position ($C\alpha$ rmsd for residues 190–193 of 3 \AA), with monomers A and B contacting opposite faces of the small molecule inhibitor (Figure S6 of the Supporting Information). Those same residues from a given monomer compared across structures overlay well [e.g., residues 190–193 of monomer B from PDB entries 4P3H and 4P2T (Figure S6 of the Supporting Information)]. The difference in the observed conformation of the C-terminal residues between monomers, but not between the same monomer across structures, is likely dictated by differences in crystal packing interactions.

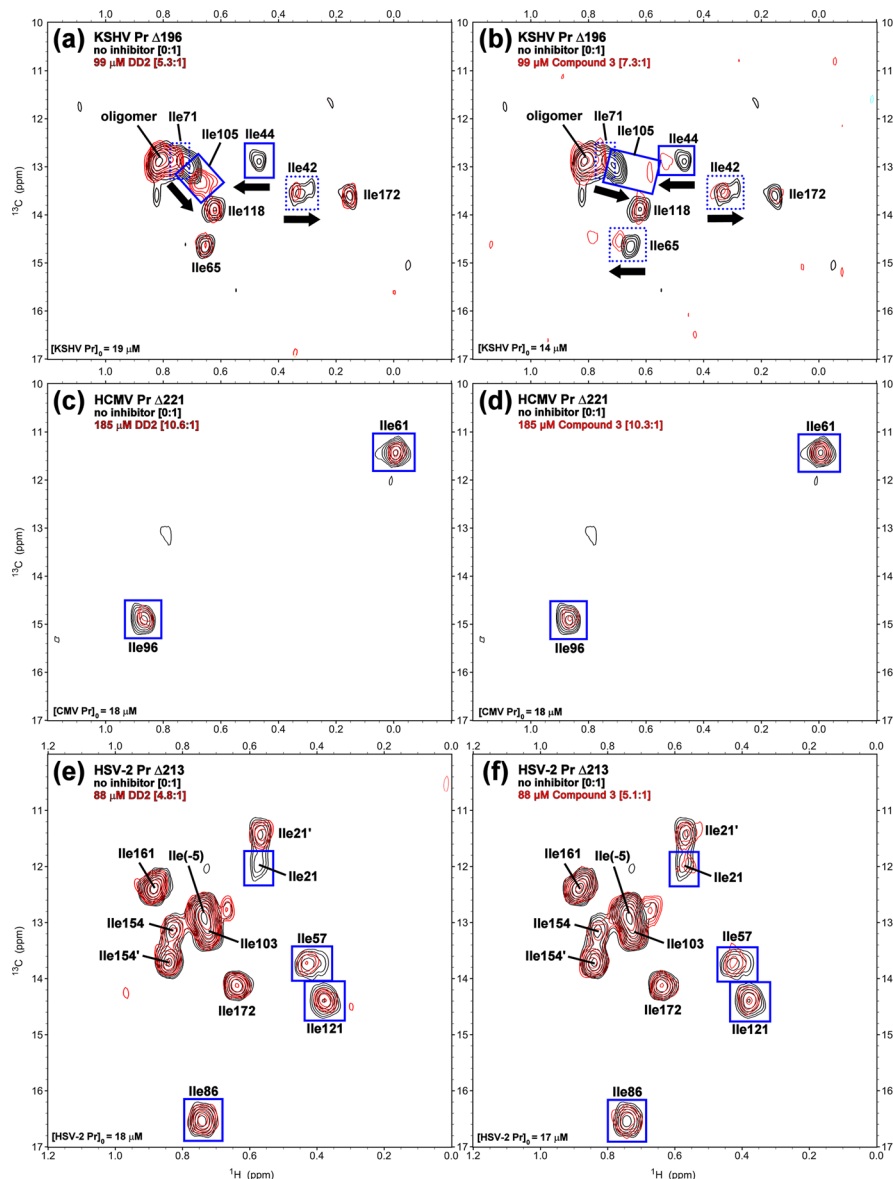


Figure 5. ^{13}C - ^1H HSQC Ile spectra in the presence of compound 3. The ^{13}C - ^1H HSQC spectra of selectively ^{13}C - ^1H [$\delta 1$ -methyl]isoleucine-labeled truncated constructs KSHV Pr $\Delta 196$ (a and b), HCMV Pr $\Delta 221$ (c and d), and HSV-2 Pr $\Delta 213$ (e and f) in the presence of 0 (black) and 5–10 molar equiv of compound 3 (red; a, c, and f) or DD2 (red; b, d, and e) indicate compound 3 and DD2 bind at the dimer interface across representative members of all three herpesvirus subfamilies.

experienced by the two monomers. The interface between monomers is largely hydrophilic and contains structural waters. The buried solvent-accessible surface areas of the monomer interfaces for the cocrystal structures of compounds 2 and 3 are 1550 and 1400 Å, respectively, while the solvent-excluded surface areas are only 670 and 615 Å, respectively. This strongly suggests the interface between monomers is purely crystallographic, consistent with NMR data showing this construct is monomeric in solution. The overall architecture of the unit cell resembled the configuration and had the same space group ($I222$) as the previously published DD2-KSHV Pr $\Delta 196$ structure (PDB entry 3NJQ) despite the use of different crystallization conditions.²⁷ Both monomer chains have a small molecule bound in the DD2 pocket at aromatic hot spot Trp109. Chain B contains an additional instance of the small molecule that acts as a crystal contact and bridges asymmetric units, as previously observed (Figure 6).²⁷ All three instances of

the inhibitor for both structures have an occupancy of 1 and average *B* factors in the range of 20–25, consistent with the *B* factor of surrounding residues.

Examination of monomer A for both cocrystal structures shows a hydrogen bond between the carboxylate bioisostere and a structural water molecule, as well as van der Waals interactions with Pro192 and the Leu193 side chain (Figure 7a,c). The partial positive charge of proline and the negative π electron density of aromatic groups such as tetrazoles have been reported to interact specifically.³⁸ The methyl of the sulfonamide in compound 3 of monomer A contacts the Leu193 side chain (Figure 7a). The larger acylsulfonamide moiety appears to help order the C-terminal residues in monomer A through van der Waals interactions between Leu193 and the methyl of the sulfonamide, as well as interactions with the Leu196 backbone. Density extending to the final residue, Leu196, is present in the cocrystal structure

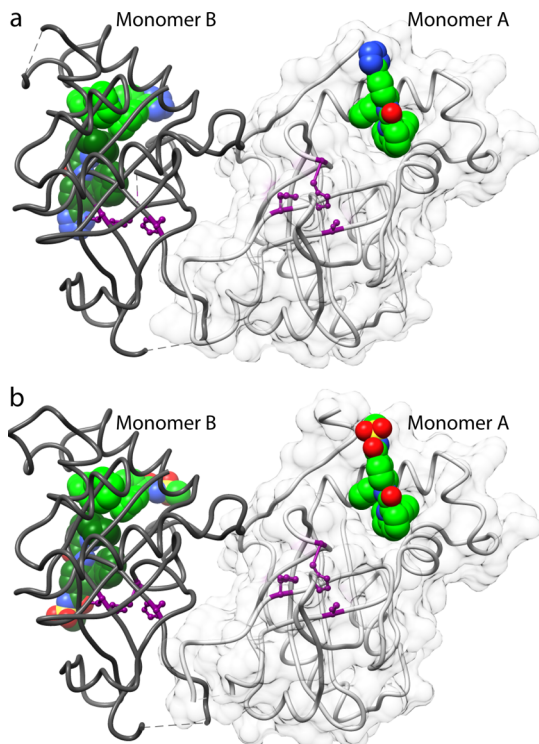


Figure 6. Asymmetric unit with the inhibitor bound. The asymmetric unit contains a crystallographic dimer of inhibited monomers (monomers A and B). The compound 2-bound structure (a) and compound 3-bound structure (b) show the major inhibitor molecules (bright green) and the bridging inhibitor molecule (dark green). The active site Ser-His-His catalytic triad is colored purple, distant from the major inhibitor molecules.

with compound 3, whereas density for residues Glu194, Thr195, and Leu196 was not present in the structure of monomer A with the smaller tetrazole moiety of compound 2. The structure of monomer B shows hydrogen bonding from the carboxylate bioisostere to the Ser191 hydroxyl for both the tetrazole and sulfonamide substituents (Figure 7b,d). In monomer A, Ser191 was positioned away from the small molecule binding pocket (Figure 7a,c). This interaction with Ser191 may be responsible for ordering the C-terminus, which could be resolved in both cocrystal structures, contrary to monomer A where it was only resolved for the compound 3 cocrystal structure. Hydrogen bonding to structural waters is also observed for the tetrazole of compound 2 in monomer B. Interactions between the remainder of the inhibitor and the pocket for both monomers mirror those previously reported for DD2 and are comprised primarily of interactions between the benzyl and cyclohexyl moieties of the small molecules and aliphatic and hydrophobic residues of the pocket.²⁷ Data collection and refinement statistics are listed in Table S1 of the Supporting Information.

Given that the small molecule inhibitors are at the interface between asymmetric units and that three distinct conformations are observed, crystal packing was analyzed to determine if one instance of the inhibitor might be more representative of solution-state binding than others. The bridging molecule (associated with monomer B) is oriented such that in the absence of the crystal lattice the benzyl and cyclohexyl rings would be largely solvent-exposed, with a total solvent-excluded surface area of just 70 Å². This would be highly unfavorable and

is not likely to exist in solution. In contrast, the inhibitor bound at Trp109 in monomer B buries 288 Å² of solvent-excluded surface area. In monomer A, the symmetry-mate bridging inhibitor molecule interacts extensively with the monomer A inhibitor and appears to severely perturb the small molecule binding pose (Figure S7 of the Supporting Information). Approximately 30% of the total surface area of the monomer A inhibitor molecule is buried by other instances of the inhibitor in the lattice, in comparison to only half of that (~15%) for the monomer B inhibitor. For these reasons, we hypothesize that the monomer B inhibitor bound in the Trp109 pocket is most representative of the solution state, not that of monomer A or the bridging molecule.

It was not immediately apparent how these structures, or the previous DD2-KSHV Pr Δ196 structure, explain the observation that only anionic replacements of the carboxylate in DD2 inhibit enzyme activity, while polar nonionic groups such as the carboxamide and ester (compounds 4 and 6, respectively) show no inhibition. To improve our understanding of solution-state binding and the observed structure–activity relationships (SARs) for DD2 and its analogues, the inhibitor-bound monomer was minimized using the Protein Local Optimization Program (PLOP) with the OPLS2005 force field (Materials and Methods). Minimization of the monomer–ligand complex alone is intended to help remove artifacts introduced by crystal packing. This modeling of monomer B predicts an interaction between cationic Arg82 and the anionic substituent of these inhibitors, with very little change in backbone or side chain positions in the pocket (Figure 8b,e and Figure S8 of the Supporting Information). Arg82–inhibitor interaction was not observed in either crystal structure or in the previous KSHV Pr Δ196–DD2 structure. Hypothesizing that this interaction could take place in solution, we examined the packing of neighboring symmetry-mate molecules in the crystal lattice and revealed how crystal packing could prevent this interaction from taking place. In monomer B, the symmetry-mate Leu140 side chain (from chain A of a neighboring asymmetric unit) sterically occludes an Arg82–compound interaction (Figure 8a,d). For monomer A, the symmetry-mate bridging inhibitor molecule interacts with Arg82 and sterically occludes interaction with the monomer A inhibitor molecule (Figure S7 of the Supporting Information). Crystallographic data for all three structures, however, suggest the Arg82 side chain is dynamic with a high average *B* factor (relative to the structure average) and density consistent with at least one alternate conformation. To test the prediction that Arg82 interacts with the anionic substituent of DD2 and its analogues, IC₅₀ values were determined for DD2, compound 2, and compound 3 with the R82Q mutant of KSHV Pr. Even with this conservative mutation, which retained potential polar interaction and the overall side chain shape, a 3–4-fold decrease in potency was observed, indicating weaker binding of KSHV Pr R82Q compared to that of the wild-type protease (Figure 8c,f and Figure S9 of the Supporting Information).

■ DISCUSSION

Small molecules that allosterically regulate protein function have been increasingly sought-after as an alternative to classical active site inhibitors.^{39–41} The homodimeric human herpesvirus proteases illustrate one such case in which small molecule allosteric modulators of activity could find extensive use in both improving our understanding of herpesvirus biology and treating infection. Because these proteases have thus far been

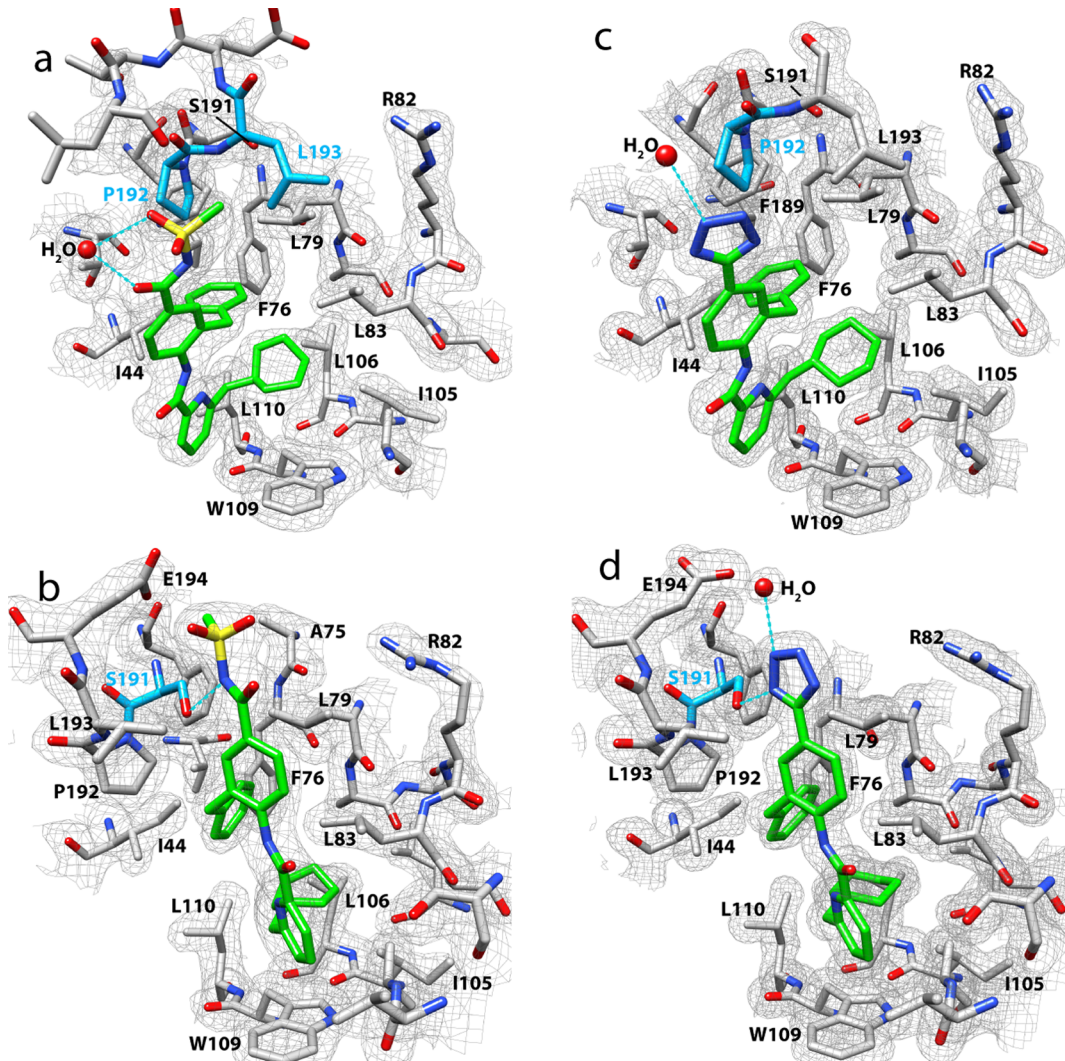


Figure 7. Compound 2 and 3 binding pockets. Compound 2 (green) in monomers A (a) and B (b) and compound 3 (green) in both monomers (c and d) bind the same largely hydrophobic pocket. The pocket is comprised primarily of aliphatic residues where binding is driven by hydrophobic interactions with the cyclohexyl and benzyl substituents of the compound. Trp109 adopts an open rotameric conformation relative to the dimeric KSHV Pr structure (PDB entry 2PBK). In monomer A, both compounds interact with Pro192 (cyan) and a structural water molecule. Compound 3 interacts extensively with Leu193 (cyan). In monomer B, both compounds hydrogen bond to the Ser191 hydroxyl, while in monomer A, Ser191 faces away from the small molecule. The mesh displays the $2F_o - F_c$ density map contoured to 1σ .

recalcitrant to noncovalent active site inhibition, likely because of their shallow and conformationally dynamic substrate binding site, we pursued allosteric inhibitors.^{12,13} Targeting protein–protein interactions with small molecules, while still a major challenge in chemical biology and drug discovery, represented an opportunity and alternative approach to regulating HHV Pr activity. The conserved allosteric link between the dimer interface and each monomer's active site allowed us to pursue a small molecule that allosterically inhibits HHV proteases from all subfamilies by targeting their dimer interfaces.

Our data support a model in which compounds 2 and 3 allosterically inhibit representatives of all three subfamilies of HHV proteases in a manner analogous to DD2 inhibition of KSHV Pr. In this model, they bind a pocket at the dimer interface, >10 Å from the active site. Binding to this site prevents C-terminal helices 5 and 6 from folding against the hydrophobic dimer interface. While these two helices are in a disordered state, the oxyanion hole of the active site, normally

formed in part by the two conserved arginines in contact with helix 6, cannot adopt the correct conformation that allows efficient proteolysis of peptide substrates to occur. Additionally, substrate binding may be prevented by conformational changes that occlude the substrate binding pocket, such as movement of loop residues 14–27 in KSHV Pr (Figure 9).²⁷ In this model, binding of compound 2 or 3 results in trapping of the inactive monomer, preventing homodimerization and thus allosterically inhibiting proteolysis across all HHV Pr subfamilies.

Via alteration of the carboxylate moiety of the parent compound, DD2, compound 2 was identified and demonstrated to have comparable or improved potency against all HHV proteases. This improvement could be caused by the larger van der Waals surface area of the tetrazole compared to the carboxylate functional group of DD2, without additional rotatable bonds, as found in compound 3. Compound 3 may exhibit IC_{50} values higher than those of DD2 due to steric or entropic effects deriving from the larger acylsulfonamide moiety.

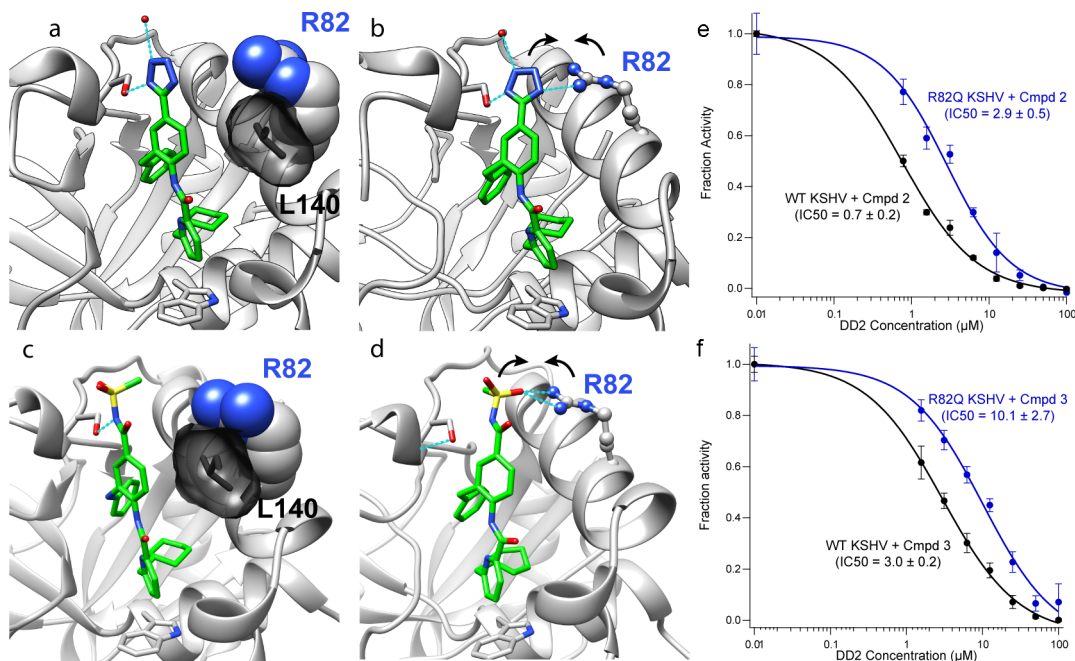


Figure 8. Compound binding mode with and without crystal packing. Models of compounds 2 and 3 were generated by minimizing the compound–monomer complex using PLOP (b and e). Arg82 is predicted to interact with the anionic carboxylate bioisostere, in contrast to the crystal structure in which a symmetry-mate Leu140 side chain prevents such interaction (a and d). IC₅₀ values determined for KSHV Pr R82Q are substantially greater (reduced potency) than those for WT KSHV Pr (c and f).

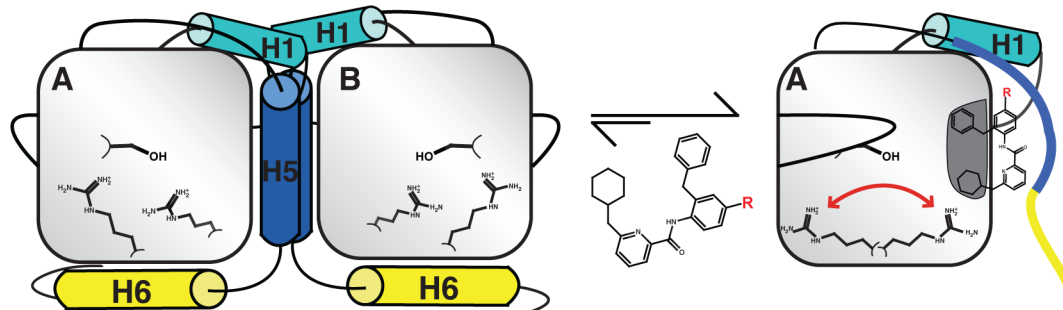


Figure 9. Model of the conserved mechanism of inhibition. Compounds 2 and 3 bind an allosteric pocket in the core of the protein preventing folding of helix 5 (H5, blue) and helix 6 (H6, yellow), “trapping” the inactive monomer (right). In contrast to the active dimer (left), when H6 is unfolded, two conserved arginines no longer stabilize the oxyanion hole (red arrow), thus preventing proteolytic activity. The active site serine is largely unperturbed; however, a loop (right) partially occludes the substrate binding cleft. R in the chemical structure represents anionic carboxylate bioisosteres.

The application of Zhang–Poorman analysis to HHV Pr family members provides a new tool for mechanism of action studies with potential inhibitors and suggests utility for the approach with other dimeric enzymes. This strictly kinetic approach is more rapid and cost-effective than NMR-based assays, with potential for use as a secondary screen in high-throughput screening campaigns for dimer disruptors. The data obtained from the kinetic analysis complement direct structural methods when they are available, as showcased here. Zhang–Poorman analysis shows that compound 2 inhibits primarily by dimer disruption of KSHV (γ), EBV (γ), and HCMV (β) proteases. Selective ^{13}C – ^1H [δ -methyl]Met labeling of KSHV Pr confirms dimer disruption, wherein slow exchange allows for the observation of distinct dimer and monomer Met197 peaks and addition of compound 2 or 3 results in a loss of the dimer resonance. Across representative proteases from all three subfamilies, selective ^{13}C – ^1H [δ -methyl]Ile data indicate

compounds 2 and 3 bind at the dimer interface in the core of the Pr monomer >10 Å from the active site.

Interestingly, nascent structure–activity relationships (SARs) for this class of inhibitors suggest a role for carboxylate or carboxylate bioisosteres in inhibiting HHV proteases. This prompted us to pursue cocrystallization studies with compounds 2 and 3 and to re-examine the DD2-KSHV $\Delta 196$ structure. Initial crystallographic results did not reveal an obvious structural explanation for this observation. After careful analysis, it became apparent that crystallographic contacts obstructed the key interaction driving the observed SAR, namely, formation of a salt bridge between Arg82 and the anionic substituent of this class of inhibitors. This interaction was predicted from computational modeling of the asymmetric unit outside of the context of the crystal lattice. A conservative mutation of Arg82 to glutamine supported the conclusion that Arg82 interacts with members of this inhibitor series. The IC₅₀ of DD2 for the R82Q mutant was roughly 3–4-fold higher than

that for the wild-type enzyme, suggesting a significantly weaker binding to the DD2 pocket. In this case, minimization of the structure without surrounding symmetry-mate molecules likely revealed a more accurate solution-state structure. This approach may be particularly important for protein–protein interaction inhibitor studies in which an exposed protein-binding interface may be involved in crystallographic contacts that are not representative of conformations in solution.

Consistent with other examples of small molecules binding at large protein surfaces, compounds **2** and **3** rely on the malleability of protein–protein interfaces, binding a cryptic pocket not apparent from apo structures.^{42,43} Strikingly, our model suggests that some conformations sampled in the dynamic and inactive monomeric states of HHV proteases are shared across subfamilies and are thus available to be trapped by compounds such as DD2, compound **2**, and compound **3**. This has broad implications for the discovery of allosteric inhibitors, indicating that highly dynamic proteins of the same family may share pockets present in states with diminished or enhanced activity that could be exploited for modulation by small molecules. This observation is consistent with and expands on prior reports using sequence conservation in large protein families to infer residue networks involved in allostery.^{44,45} Many examples of both homo- and heterodimeric complexes that undergo conformational changes upon dimerization are detailed in the literature and could be subject to allosteric regulation, especially those in which one or both partners are in part intrinsically unfolded.^{46–49}

In summary, we have established kinetic and structural methods for analysis of representative members of all three subfamilies of the HHV proteases. In doing so, we showed that compound **2** has improved potency and allosterically inhibits HHV proteases broadly by disrupting dimerization. At 1.45 Å resolution, the cocrystal structure with compound **2** bound provides the highest-resolution structure to date of the KSHV Pr monomer bound to a protein–protein interaction inhibitor. SAR data and modeling inform our interpretation of cocrystallization studies as well as previously published data for this class of inhibitors and will aid in future screening and design against this family of targets. These analyses and discoveries provide an approach for the identification of small molecules that allosterically regulate protein activity by targeting protein–protein interactions.

ASSOCIATED CONTENT

Supporting Information

Additional data and graphics to aid in the interpretation of this work. This material is available free of charge via the Internet at <http://pubs.acs.org>.

AUTHOR INFORMATION

Corresponding Author

*E-mail: charles.craik@ucsf.edu. Phone: (415) 476-8146.

Funding

This work was supported by the National Center for Research Resources and the National Center for Advancing Translational Sciences, National Institutes of Health (NIH), through UCSF Clinical and Translational Science Institute (CTSI) Grants UL1 TR000004 and UL1 RR024131. This work was also funded in part by grants from the NIH (R01-AI090592 and P50-GM082250), the National Cancer Institute, and the Helen Diller Family Comprehensive Cancer Center (P30 CA 82103-

13). J.E.G. was supported by NIH Structural Biology Training Grant GM008284 and the National Science Foundation Graduate Research fellowship program (1144247).

Notes

The authors declare no competing financial interest.

ACKNOWLEDGMENTS

We thank Prof. Geeta Narlikar, Dr. Brian Metcalf, and Prof. R. Kip Guy for useful discussions and technical support.

ABBREVIATIONS

ACC, 7-amino-4-carbamoylmethylcoumarin; DD2, dimer disruptor 2; DTT, dithiothreitol; EBV Pr, Epstein-Barr virus protease; HCMV Pr, human cytomegalovirus protease; HHV Pr, human herpesvirus protease; HSQC, heteronuclear single-quantum coherence; HSV-2 Pr, herpes simplex virus 2 protease; KSHV Pr, Kaposi's sarcoma-associated herpesvirus protease; MCMV, murine cytomegalovirus; rmsd, root-mean-square deviation; SAR, structure–activity relationship; tBu, *tert*-butylglycine; VZV, Varicella Zoster virus.

REFERENCES

- (1) Tong, L. (2002) Viral proteases. *Chem. Rev.* **102**, 4609–4626.
- (2) Coen, D. M., and Schaffer, P. A. (2003) Antiherpesvirus drugs: A promising spectrum of new drugs and drug targets. *Nat. Rev. Drug Discovery* **2**, 278–288.
- (3) Gao, M., Matusick-Kumar, L., Hurlburt, W., DiTusa, S. F., Newcomb, W. W., Brown, J. C., McCann, P. J., III, Deckman, I., and Colonna, R. J. (1994) The protease of herpes simplex virus type 1 is essential for functional capsid formation and viral growth. *J. Virol.* **68**, 3702–3712.
- (4) Jiang, X. H., Gong, H., Chen, Y. C., Vu, G. P., Trang, P., Zhang, C. Y., Lu, S. W., and Liu, F. Y. (2012) Effective inhibition of cytomegalovirus infection by external guide sequences in mice. *Proc. Natl. Acad. Sci. U.S.A.* **109**, 13070–13075.
- (5) Waxman, L., and Darke, P. L. (2000) The herpesvirus proteases as targets for antiviral chemotherapy. *Antiviral Chem. Chemother.* **11**, 1–22.
- (6) Marnett, A. B., Nomura, A. M., Shimba, N., Ortiz de Montellano, P. R., and Craik, C. S. (2004) Communication between the active sites and dimer interface of a herpesvirus protease revealed by a transition-state inhibitor. *Proc. Natl. Acad. Sci. U.S.A.* **101**, 6870–6875.
- (7) Borthwick, A. D., Crame, A. J., Ertl, P. F., Exall, A. M., Haley, T. M., Hart, G. J., Mason, A. M., Pennell, A. M., Singh, O. M., Weingarten, G. G., and Woolven, J. M. (2002) Design and synthesis of pyrrolidine-5,5-trans-lactams (5-oxohexahydropyrrolo[3,2-b]pyrroles) as novel mechanism-based inhibitors of human cytomegalovirus protease. Part 2. Potency and chirality. *J. Med. Chem.* **45**, 1–18.
- (8) Borthwick, A. D., Exall, A. M., Haley, T. M., Jackson, D. L., Mason, A. M., and Weingarten, G. G. (2002) Pyrrolidine-5,5-trans-lactams as novel mechanism-based inhibitors of human cytomegalovirus protease. Part 3: Potency and plasma stability. *Bioorg. Med. Chem. Lett.* **12**, 1719–1722.
- (9) Borthwick, A. D., Weingarten, G., Haley, T. M., Tomaszewski, M., Wang, W., Hu, Z., Bedard, J., Jin, H., Yuen, L., and Mansour, T. S. (1998) Design and synthesis of monocyclic β -lactams as mechanism-based inhibitors of human cytomegalovirus protease. *Bioorg. Med. Chem. Lett.* **8**, 365–370.
- (10) Gopalsamy, A., Lim, K., Ellingboe, J. W., Mitsner, B., Nikitenko, A., Upeslacis, J., Mansour, T. S., Olson, M. W., Bebernitz, G. A., Grinberg, D., Feld, B., Moy, F. J., and O'Connell, J. (2004) Design and syntheses of 1,6-naphthalene derivatives as selective HCMV protease inhibitors. *J. Med. Chem.* **47**, 1893–1899.
- (11) Ogilvie, W., Bailey, M., Poupart, M. A., Abraham, A., Bhavsar, A., Bonneau, P., Bordeleau, J., Bousquet, Y., Chabot, C., Duceppe, J. S., Fazal, G., Goulet, S., Grand-Maitre, C., Guse, I., Halmos, T., Lavallee,

- P., Leach, M., Malenfant, E., O'Meara, J., Plante, R., Plouffe, C., Poirier, M., Soucy, F., Yoakim, C., and Deziel, R. (1997) Peptidomimetic inhibitors of the human cytomegalovirus protease. *J. Med. Chem.* 40, 4113–4135.
- (12) Lazic, A., Goetz, D. H., Nomura, A. M., Marnett, A. B., and Craik, C. S. (2007) Substrate modulation of enzyme activity in the herpesvirus protease family. *J. Mol. Biol.* 373, 913–923.
- (13) Reiling, K. K., Pray, T. R., Craik, C. S., and Stroud, R. M. (2000) Functional consequences of the Kaposi's sarcoma-associated herpesvirus protease structure: Regulation of activity and dimerization by conserved structural elements. *Biochemistry* 39, 12796–12803.
- (14) Batra, R., Khayat, R., and Tong, L. (2001) Molecular mechanism for dimerization to regulate the catalytic activity of human cytomegalovirus protease. *Nat. Struct. Biol.* 8, 810–817.
- (15) LaPlante, S. R., Bonneau, P. R., Aubry, N., Cameron, D. R., Deziel, R., Grand-Maitre, E., Plouffe, C., Tong, L., and Kawai, S. H. (1999) Characterization of the human cytomegalovirus protease as an induced-fit serine protease and the implications to the design of mechanism-based inhibitors. *J. Am. Chem. Soc.* 121, 2974–2986.
- (16) Nomura, A. M., Marnett, A. B., Shimba, N., Dotsch, V., and Craik, C. S. (2005) Induced structure of a helical switch as a mechanism to regulate enzymatic activity. *Nat. Struct. Mol. Biol.* 12, 1019–1020.
- (17) Qiu, X., Janson, C. A., Culp, J. S., Richardson, S. B., Debouck, C., Smith, W. W., and Abdel-Meguid, S. S. (1997) Crystal structure of varicella-zoster virus protease. *Proc. Natl. Acad. Sci. U.S.A.* 94, 2874–2879.
- (18) Buisson, M., Hernandez, J. F., Lascoux, D., Schoehn, G., Forest, E., Arlaud, G., Seigneurin, J. M., Ruigrok, R. W., and Burmeister, W. P. (2002) The crystal structure of the Epstein-Barr virus protease shows rearrangement of the processed C terminus. *J. Mol. Biol.* 324, 89–103.
- (19) Chen, P., Tsuge, H., Almassy, R. J., Gribskov, C. L., Katoh, S., Vanderpool, D. L., Margosiak, S. A., Pinko, C., Matthews, D. A., and Kan, C. C. (1996) Structure of the human cytomegalovirus protease catalytic domain reveals a novel serine protease fold and catalytic triad. *Cell* 86, 835–843.
- (20) Tong, L., Qian, C., Massariol, M. J., Bonneau, P. R., Cordingley, M. G., and Lagace, L. (1996) A new serine-protease fold revealed by the crystal structure of human cytomegalovirus protease. *Nature* 383, 272–275.
- (21) Shieh, H. S., Kurumbail, R. G., Stevens, A. M., Stegeman, R. A., Sturman, E. J., Pak, J. Y., Wittwer, A. J., Palmier, M. O., Wiegand, R. C., Holwerda, B. C., and Stallings, W. C. (1996) Three-dimensional structure of human cytomegalovirus protease. *Nature* 383, 279–282.
- (22) Pray, T. R., Nomura, A. M., Pennington, M. W., and Craik, C. S. (1999) Auto-inactivation by cleavage within the dimer interface of Kaposi's sarcoma-associated herpesvirus protease. *J. Mol. Biol.* 289, 197–203.
- (23) Pray, T. R., Reiling, K. K., Demirjian, B. G., and Craik, C. S. (2002) Conformational change coupling the dimerization and activation of KSHV protease. *Biochemistry* 41, 1474–1482.
- (24) Shimba, N., Nomura, A. M., Marnett, A. B., and Craik, C. S. (2004) Herpesvirus protease inhibition by dimer disruption. *J. Virol.* 78, 6657–6665.
- (25) Hoog, S. S., Smith, W. W., Qiu, X., Janson, C. A., Hellmig, B., McQueney, M. S., O'Donnell, K., O'Shannessy, D., DiLella, A. G., Debouck, C., and Abdel-Meguid, S. S. (1997) Active site cavity of herpesvirus proteases revealed by the crystal structure of herpes simplex virus protease/inhibitor complex. *Biochemistry* 36, 14023–14029.
- (26) Schmidt, U., and Darke, P. L. (1997) Dimerization and activation of the herpes simplex virus type 1 protease. *J. Biol. Chem.* 272, 7732–7735.
- (27) Lee, G. M., Shahian, T., Baharuddin, A., Gable, J. E., and Craik, C. S. (2011) Enzyme Inhibition by Allosteric Capture of an Inactive Conformation. *J. Mol. Biol.* 411, 999–1016.
- (28) Nomura, A. M., Marnett, A. B., Shimba, N., Dotsch, V., and Craik, C. S. (2006) One functional switch mediates reversible and irreversible inactivation of a herpesvirus protease. *Biochemistry* 45, 3572–3579.
- (29) Craik, C. S., and Shahian, T. (2012) A screening strategy for trapping the inactive conformer of a dimeric enzyme with a small molecule inhibitor. *Methods Mol. Biol.* 928, 119–131.
- (30) Shahian, T., Lee, G., Lazic, A., Arnold, A., Velusamy, P., Roels, C. M., Guy, R. K., and Craik, C. S. (2009) Inhibition of a Viral Enzyme by a Small Molecule Dimer Disruptor. *Nat. Chem. Biol.* 9, 640–646.
- (31) Zhang, Z. Y., Poorman, R. A., Maggiora, L. L., Heinrikson, R. L., and Kezdy, F. J. (1991) Dissociative Inhibition of Dimeric Enzymes: Kinetic Characterization of the Inhibition of HIV-1 Protease by Its COOH-Terminal Tetrapeptide. *J. Biol. Chem.* 266, 15591–15594.
- (32) Harris, J. L., Backes, B. J., Leonetti, F., Mahrus, S., Ellman, J. A., and Craik, C. S. (2000) Rapid and general profiling of protease specificity by using combinatorial fluorogenic substrate libraries. *Proc. Natl. Acad. Sci. U.S.A.* 97, 7754–7759.
- (33) Buisson, M., Valette, E., Hernandez, J. F., Baudin, F., Ebel, C., Morand, P., Seigneurin, J. M., Arlaud, G. J., and Ruigrok, R. W. (2001) Functional determinants of the Epstein-Barr virus protease. *J. Mol. Biol.* 311, 217–228.
- (34) Bowman, M. J., Byrne, S., and Chmielewski, J. (2005) Switching between allosteric and dimerization inhibition of HIV-1 protease. *Chem. Biol.* 12, 439–444.
- (35) Jacobson, M. P., Friesner, R. A., Xiang, Z. X., and Honig, B. (2002) On the role of the crystal environment in determining protein side-chain conformations. *J. Mol. Biol.* 320, 597–608.
- (36) Jacobson, M. P., Kaminski, G. A., Friesner, R. A., and Rapp, C. S. (2002) Force field validation using protein side chain prediction. *J. Phys. Chem. B* 106, 11673–11680.
- (37) Li, X., Jacobson, M. P., and Friesner, R. A. (2004) High-resolution prediction of protein helix positions and orientations. *Proteins* 55, 368–382.
- (38) Zondlo, N. J. (2013) Aromatic-Proline Interactions: Electronically Tunable CH/π Interactions. *Acc. Chem. Res.* 46, 1039–1049.
- (39) Wells, J. A., and McClendon, C. L. (2007) Reaching for high-hanging fruit in drug discovery at protein-protein interfaces. *Nature* 450, 1001–1009.
- (40) Kar, G., Keskin, O., Gursoy, A., and Nussinov, R. (2010) Allostery and population shift in drug discovery. *Curr. Opin. Pharmacol.* 10, 715–722.
- (41) Lee, G. M., and Craik, C. S. (2009) Trapping moving targets with small molecules. *Science* 324, 213–215.
- (42) Sundberg, E. J., and Mariuzza, R. A. (2000) Luxury accommodations: The expanding role of structural plasticity in protein-protein interactions. *Structure* 8, R137–R142.
- (43) Teague, S. J. (2003) Implications of protein flexibility for drug discovery. *Nat. Rev. Drug Discovery* 2, 527–541.
- (44) Suel, G. M., Lockless, S. W., Wall, M. A., and Ranganathan, R. (2003) Evolutionarily conserved networks of residues mediate allosteric communication in proteins (vol 10, pg 59, 2003). *Nat. Struct. Biol.* 10, 232.
- (45) Reynolds, K. A., McLaughlin, R. N., and Ranganathan, R. (2011) Hot Spots for Allosteric Regulation on Protein Surfaces. *Cell* 147, 1564–1575.
- (46) Yuan, Y., Zhao, W., Wang, X., Gao, Y., Niu, L., and Teng, M. (2012) Dimeric Sfh3 has structural changes in its binding pocket that are associated with a dimer-monomer state transformation induced by substrate binding. *Acta Crystallogr. D69*, 313–323.
- (47) McDonald, C. B., Seldeen, K. L., Deegan, B. J., Lewis, M. S., and Farooq, A. (2008) Grb2 adaptor undergoes conformational change upon dimerization. *Arch. Biochem. Biophys.* 475, 25–35.
- (48) Demchenko, A. P. (2001) Recognition between flexible protein molecules: Induced and assisted folding. *J. Mol. Recognit.* 14, 42–61.
- (49) Dyson, H. J., and Wright, P. E. (2002) Coupling of folding and binding for unstructured proteins. *Curr. Opin. Struct. Biol.* 12, 54–60.